AIAA-91-1775

Length Scales of Turbulence Near a Free Surface

R. Handler, J. Swearingen, T. Swean
Naval Research Laboratory
Washington, DC

R. Leighton
Science Applications, Inc.
McLean, VA

AIAA 22nd Fluid Dynamics, Plasmadynamics & Lasers Conference
June 24-26, 1991 / Honolulu, HI

AIAA-91-1775-CP

LENGTH SCALES OF TURBULENCE NEAR A FREE SURFACE

R.A. Handler,† J.D. Swearingen,† T.F. Swean, Jr.,†† R.I. Leighton*
Center For Advanced Space Sensing
Naval Research Laboratory
Washington, D.C. 20375-5000

ABSTRACT

Two-point correlations, energy spectra, and length scales are examined in the vicinity of a free surface, modeled as a shear-free boundary in a direct numerical simulation of open channel flow. The length scale results indicate that a typical eddy is flattened as it interacts with the surface. The scales associated with the vertical component of velocity seem to determine the extent of the source layer described in the Hunt-Graham model. The energy spectra show qualitative agreement with the model, though higher resolution calculations will be required to make more quantitative comparisons. Additionally, the proximity of the free surface to the bottom solid wall of the channel evidences itself as a wall-layer streaky structure which persists to a noticeably greater distance away from the wall. Some speculations are offered to explain this effect.

NOMENCLATURE

h	= channel height
k	= turbulent kinetic energy
ℓ^*	= ν/u_τ, viscous length scale
Re_h	= $\overline{U}_s h/\nu$, Reynolds number
R^*	= $u_\tau h/\nu$, wall Reynolds number
R_θ	= $U_\infty \theta/\nu$, momentum thickness Reynolds number
t^*	= ν/u_τ^2, viscous timescale
$\mathbf{U}$	= instantaneous velocity vector
U_i	= instantaneous velocity component
u_i	= fluctuating velocity component
u_τ	= $\sqrt{\tau_w/\rho}$, friction velocity
λ_{ij}	= turbulent microscale
Λ_{ij}	= turbulent macroscale
R_{ij}	= two-point correlation tensor
x_i	= coordinate direction
x_i^+	= $x_i u_\tau/\nu$
$\overline{(\ )}$	= averaged quantity
Φ_{ij}	= specral density
κ_1	= streamwise wavenumber
ν	= kinematic viscosity
ρ	= density
θ	= momentum thickness
τ_w	= shear stress
$\mathbf{\Omega}$	= instantaneous vorticity vector
Ω_i	= instantaneous vorticity component

Subscripts

i	= 1, 2, 3, coordinate directions
s	= value at free surface
∞	= value in free stream
w	= value at wall

1. INTRODUCTION

The study of the structure of turbulence near a free surface is obviously important to our understanding of the complex interaction of the atmosphere and upper ocean. It is also of fundamental relevance to the wall-bounded turbulence problem, since it isolates the boundary influence on turbulent fluctuations from the turbulence production mechanism at the wall. The first detailed experiment which addressed itself to this particular problem was that of Uzkan and Reynolds[1] (UR). They passed grid generated homogeneous turbulence over a wall which moved with the mean flow and therefore generated no mean shear at the boundary. They found that the streamwise turbulence intensity near the shear-free boundary did not peak as it does near a stationary solid wall, but instead decreased monotonically from its free stream value to zero at the boundary. Later, Thomas and Hancock[2] (TH) performed a similar experiment at a Reynolds number about 20 times greater than that of UR and found that the intensity of the streamwise component *increases* as the boundary is approached.

The discrepancy between these two results was explained satisfactorily by Hunt and Graham[3] (HG) who proposed a two layer model for the interaction. At high turbulent Reynolds numbers there exists a thin viscous layer near the wall embedded in a larger *source* layer. The source layer should be roughly the size of the integral length scale of the free stream turbulence and exists essentially because of the no mass-flux condition at the boundary. Their theory predicts a redistribution of turbulent energy in the source layer

---

†Mechanical Engineer, NRL,
††Research Mechanical Engineer, NRL, Mem. AIAA
*Research Scientist, SAIC, McLean, VA, 22102

from the vertical component of velocity to the streamwise and spanwise components. The UR result was easily explained since, at the low Reynolds number of their experiment, the viscous layer dominated the region near the surface and the turbulence was accordingly damped. At the higher Reynolds number of the TH experiment, the source layer dominated and the redistribution of the turbulence behaved according to the HG model. Many of these results were later confirmed by the large eddy simulations of Biringen and Reynolds[4]. Recently, Brumley and Jirka[5] (BJ) presented results for experiments in which homogeneous turbulence interacted with a free surface. Their results agreed reasonably well with a modified form of the HG model.

The simulations performed here were designed to represent as closely as possible the physics of free surface/turbulence interaction in which the effects of surface waves can be safely neglected. For this purpose, fully developed turbulence between a solid wall and a free surface is simulated. The physical processes represented by these simulations differ in some important respects from processes involved in the physical experiments noted above. First, in these simulations, no viscous layer can develop since u_1 and u_3, the fluctuating streamwise and spanwise velocity components, are not forced to zero as in the UR and TH experiments. In fact, even in the BJ experiments a viscous layer developed near the surface due to the presence of surface contaminants. Secondly, in these simulations, the turbulence impinging on the free surface is not isotropic since it is being generated at a solid wall. It is evident that the solid wall is acting as a generator of anisotropic turbulence which is then convected toward the free surface. Lastly, it is possible to examine the question of the influence, if any, of the free surface on the turbulent structure at the solid surface boundary. In this work two-point correlations, energy spectra, and turbulent length scales will be examined in an effort to investigate the turbulent structure near a free surface in the absence of surface waves.

2. DIRECT NUMERICAL SIMULATION

The incompressible three-dimensional Navier-Stokes equations are solved for initial and boundary conditions approximating a turbulent open channel flow of water at a Reynolds number, Re_h, based on the channel height, h, and the mean velocity at the free surface, $\overline{U_s}$, of 2340. The notation x_1, x_2, and x_3 is used to denote the streamwise, wall-normal, and spanwise coordinates respectively. The governing equations, formulated in the manner suggested by Orszag and Patera[6] and later implemented in a simpler form by Kim, Moin and Moser[7], consist of a fourth order equation for the vertical velocity, U_2 :

$$\left(\frac{\partial\nabla^2}{\partial t}-\frac{\nabla^4}{Re_h}\right)U_2=\left(\frac{\partial^2}{\partial x_1^2}+\frac{\partial^2}{\partial x_3^2}\right)(\mathbf{U}\times\mathbf{\Omega})_2 - \frac{\partial}{\partial x_2}\left(\frac{\partial}{\partial x_1}(\mathbf{U}\times\mathbf{\Omega})_3+\frac{\partial}{\partial x_3}(\mathbf{U}\times\mathbf{\Omega})_1\right), \quad (1)$$

and a second order equation for the vertical vorticity, Ω_2:

$$\left(\frac{\partial}{\partial t}-\frac{\nabla^2}{Re_h}\right)\Omega_2=\frac{\partial}{\partial x_3}(\mathbf{U}\times\mathbf{\Omega})_1-\frac{\partial}{\partial x_1}(\mathbf{U}\times\mathbf{\Omega})_3, \quad (2)$$

where all variables are made non-dimensional by h and the initial value of $\bar{U}_s$. Here, the instantaneous velocity vector is given by $\mathbf{U}$ and the instantaneous vorticity vector is defined by $\mathbf{\Omega}=(\nabla\times\mathbf{U})$. Following the solution of equations 1 and 2, the streamwise and spanwise velocity components, U_1 and U_3, are recovered from the incompressibility condition.

The equations of motion are solved in Fourier-Chebyshev space where Fourier modes are employed in the horizontal plane and Chebyshev modes in the wall normal direction. The calculations are performed on a $64\times65\times48$ grid in x_1, x_2, x_3 respectively. With the geometry scaled by the channel height, the streamwise, vertical, and transverse dimensions of the channel are 4π, 1, and $3\pi/2$ respectively. In terms of the viscous parameters consisting of the friction velocity, u_τ, and the kinematic viscosity, ν, the domain is $1684\ell^*\times134\ell^*\times632\ell^*$ and the Reynolds number, R^*, is 134. To facilitate substantive qualitative comparisons with the wall-bounded turbulence problem, a companion calculation for a closed channel flow is utilized. For reasons of economy, this calculation is at half the wall-normal resolution of the open channel case and is at a somewhat lower Reynolds number, $R^*=125$. Nevertheless the behavior of these data for all aspects examined is identical to that reported by KMM.

The boundary conditions utilized are periodic on all dependent variables in the streamwise and spanwise directions. No-slip conditions are used at the channel bottom while the free surface is approximated as a rigid, free-slip surface with vanishing shear. The shear-free rigid lid condition is an approximation to the exact free surface condition which is valid at low Froude number for a surface free of any contaminants. Leighton *et al.*[8] have estimated the surface displacement *a posteriori* from the results of the simulation using the channel height, $h=0.04m$, from the experiments of Komori *et al.*[9] . For these conditions the rms surface deflections are expected to be approximately $1.6\times10^{-4}m$ $(0.004h)$ and are clearly negligible as observed in the laboratory experiments. The boundary conditions at the solid wall ($x_2=0$) and the free surface ($x_2=1$) are:

$$U_1 = U_2 = U_3 = 0; x_2 = 0, \quad (3)$$

and

$$\frac{\partial U_1}{\partial x_2} = \frac{\partial U_3}{\partial x_2} = U_2 = 0; x_2 = 1. \quad (4)$$

The code developed for the simulation is designed to run on the CRAY X-MP/24 computer at the Naval Research Laboratory and requires approximately 10^{-5} CPU seconds per timestep per grid point. After the wall shear stress achieved a statistically steady behavior, 42 realizations of the instantaneous velocity data were saved during a time interval of approximately $4000t^*$ where $t^* = \nu/u_\tau^2$. Statistics were obtained by averaging in the streamwise and spanwise directions as well as over all realizations. Swean *et al.*[10] find good agreement between these simulations and open channel flow experiments.

3. TWO-POINT CORRELATIONS AND ENERGY SPECTRA

The turbulent structure near the free surface is revealed in some detail by examining the two-point correlations and energy spectra at different depths below the surface. The two-point correlation function, R_{ij}, is defined by :

$$R_{ij}(\Delta x_1, \Delta x_3, x_2, x_2') = \frac{\overline{u_i(x_1, x_3, x_2) u_j(x_1', x_3', x_2')}}{\sqrt{\overline{u_i^2}\ \overline{u_j^2}}}, \quad (5)$$

where, $x_j' = x_j + \Delta x_j$, j=1,3. Here, only the properties of R_{ij} for which $x_2 = x_2'$ and $i = j$ will be described. These correlations were computed by averaging over all flow realizations and all flow symmetries (see Sirovich[11]). Figure 1 shows a comparison of the streamwise correlations for open and closed channel flows at several x_2 locations. Note that in each figure a secondary axis is given showing the correlation length in terms of wall variables, i.e. Δx_1^+ for this case. In the region close to the bottom solid wall ($0 < x_2 < 0.5$; $0 < x_2^+ < 68$) the streamwise correlations are virtually identical for all three velocity components. As an example, note the similarity between the correlations at $x_2 = 0.071$ for open channel flow with those of closed channel flow at $x_2 = 0.076$. The only notable difference is a somewhat longer streamwise correlation length for u_1 in the open channel case. At distances farther from the wall, however, the differences between the two flows become increasingly more pronounced. As the free surface is approached, two trends are evident. First, the streamwise distance at which $R_{33}(\Delta x_1, 0, x_2)$, (subsequently denoted $R_{33}(\Delta x_1)$) attains its minimum value increases as the free surface is approached. For example, at $x_2 = 0.524$, the minimum occurs at $\Delta x_1 \simeq 1.34$ and as the free surface is approached this increases roughly 17% to $\Delta x_1 \simeq 1.57$. For the closed channel case, however, this distance undergoes virtually no change as x_2 varies from 0.572 to the centerline. Secondly, we observe that the streamwise correlation length of the vertical component of velocity in the open channel case, which may be loosely defined by the first zero crossing, decreases significantly between $x_2 = 0.524$, where no zero crossing exists, and $x_2 = 0.952$ where it attains a value of $\Delta x_1 \simeq 0.75$. In the closed channel case this scale also decreases, but not nearly as rapidly as in open channel flow where there appears to be a clearer separation between $R_{22}(\Delta x_1)$ and $R_{33}(\Delta x_1)$ near the free surface. In Fig. 2 the corresponding results for the spanwise correlations, $R_{jj}(\Delta x_3)$, are shown for both cases. As in the streamwise results, close to the wall there appear to be no significant differences between these flows. Farther from the wall ($x_2 \geq 0.5$), it is evident that the correlation length for the u_2 component in the open channel flow is significantly smaller than those for the other two velocity components. This behavior is not evident for the closed channel case in this same region. Again, as with the streamwise correlation length results, there is a clear separation between $R_{22}(\Delta x_3)$ and $R_{33}(\Delta x_3)$ as the free surface is approached. One feature of note is the existence of a discernable local minimum in the spanwise correlation of the streamwise velocity component out to normal locations as large as $x_2 \simeq 0.8$ (i.e., ≈ 108 viscous lengths) in the open channel case. This indicates a considerable persistence of a spanwise periodic structure in the flow which will be discussed in more detail in Section 5.

Energy spectra, Φ_{ij}, as a function of the streamwise wavenumber, κ_1, are shown in Fig. 3 for two different surface normal locations in close proximity to the free surface boundary ($x_2 = 0.978$ and 0.952). Additionally, a third energy spectrum at $x_2 = 0.798$ is given in each plot as a reference condition. Examination of the turbulence intensity profiles (refer to the Fig. 7 discussed later) at this location indicates that free surface effects will be negligible. The $\Phi_{11}(\kappa_1)$ spectra show that very near the free surface, the energy at low wavenumbers remains unchanged. However, for the intermediate band ($2 < \kappa_1 < 10$) a small increase in energy is evident. There is no change in the spectra at high wavenumbers. These features are quite consistent with the HG predictions. From the $\Phi_{22}(\kappa_1)$ spectra it is quite evident that, as the free surface is approached, the energy at low wavenumbers decreases more rapidly than at high wavenumbers. This is also consistent with HG. However, it is to be noted that the HG model predicts that the $\Phi_{22}(\kappa_1)$ spectrum far from the boundary will merge with the spectra near the free surface at a wavenumber of order $2\pi/\Delta x_2$, where Δx_2 is the vertical distance from

the free surface. This is effectively due to the cutting off of eddies smaller than Δx_2 by the presence of the surface. In these calculations, however, the minimum resolvable streamwise length scale dictated by the grid spacing is $4\pi/64 = 0.196$, which is in fact of the same order as the source layer. It is evident that higher resolution will be required to resolve these effects. Nevertheless, the basic structure of $\Phi_{22}(\kappa_1)$ is suggestive of this kind of wavenumber cutoff behavior. The $\Phi_{33}(\kappa_1)$ spectra show some increase in energy at low wavenumbers as the free surface is approached, but virtually no change for $k_1 > 3$. These observations are also qualitatively consistent with HG.

4. MACRO AND MICROSCALES

Turbulent flows are known to contain a wide range of length scales; here we examine both the turbulent macroscales and microscales. The macroscale can be considered the length scale that represents the size of a typical energy containing eddy which is eventually broken up and dissipated by viscosity at smaller scales[12]. The microscale, though not the smallest length scale in the flow, can be thought of as an average length within which most of the energy dissipation occurs. In high Reynolds number flows there is a large separation between these two scales, but in the current computations this separation is not large.

The microscale, λ, corresponding to velocity component u_j in direction x_i is defined by:

$$\lambda_{ij}^2 = -2/\frac{\partial^2 R_{jj}(x_i)}{\partial^2 x_i}\bigg|_{x_i=0} . \qquad (6)$$

If the turbulence is homogeneous in direction x_i then it can be shown that an equivalent definition is :

$$\lambda_{ij}^2 = \overline{u_j^2}/\overline{\left(\frac{\partial u_j}{\partial x_i}\right)^2} . \qquad (7)$$

The x_1 and x_3 microscales are computed using both definitions given above and nominally produce identical results. The macroscale Λ is defined by :

$$\Lambda_{ij} = \int_0^\infty R_{jj}(x_i)dx_i . \qquad (8)$$

It should be noted that in some circumstances, particularly for the streamwise velocity component, the correlation function $R_{jj}(\Delta x_1)$ does not decay sufficiently at the end of the computational domain so that the macroscale given by (8) may underestimate the true eddy length scale. Also, since quasi-periodic structures exist close to the wall with their periodicity primarily in the spanwise x_3 direction, $R_{jj}(\Delta x_3)$ can be negative. This also has the effect of producing a macroscale which underestimates the length of the largest eddy structures near the wall. For these reasons, the microscales reported below may actually be larger in some cases than the macroscales. This is simply an artifact of the method used here. A better estimate for the macroscales can be had in some cases by using the length associated with the second zero crossing of the correlation function.

Figure 4 shows the results of the calculation of the streamwise macroscale, Λ_1 (i.e Λ_{1j}), and the spanwise macroscale, Λ_3, for both the open and closed channel cases. Recall that the solid wall is at $x_2 = 0$ and the free surface (or centerline) is at $x_2 = 1$. The scales are nominally given in terms of outer units (i.e., channel height) since conversion to wall variables can easily be obtained by multipyling by 135 in the open channel case and 125 for the closed channel. For the streamwise macroscales, significant differences between these two cases are apparent in the rather large region $0.4 < x_2 < 1.0$. Here, the most notable observation is that the u_3 velocity component Λ_1 length scale changes by a factor of approximately three (≈ 0.60 at the open channel free surface relative to 0.19 at the centerline of the closed channel). For the streamwise velocity component, Λ_1 differs only slightly at the free surface from the closed channel centerline value (1.4 vs. 1.14); however, there is a substantially different behavior in how these final values are attained. The closed channel length scale smoothly achieves an asymptotic value of order one at the centerline, whereas the behavior near the free surface resembles that observed near the solid boundary (i.e., a peak at some distance from the boundary indicative of the source layer thickness). The free surface effects on the spanwise macroscales, Λ_3, are confined to a smaller region ($0.8 < x_2 < 1.0$) than those on the streamwise macroscales. Substantial differences are again observed between the values attained at the free surface relative to those at the closed channel centerline. Both the u_1 and u_2 component macroscales differ by a factor of about two with the u_1 scale larger and the u_2 scale correspondingly smaller at the free surface.

In Fig. 5 the microscale results are compared for the open and closed channel flows. Trends similar to those observed for the macroscale results of Fig. 4 are apparent. The streamwise scale, λ_1, of the u_3 component is larger at the free surface than at the closed channel centerline (0.40 vs. 0.29); whereas, λ_1 for the u_2 component is somewhat lower (0.21 vs. 0.27). Similar to the spanwise macroscale results, the spanwise microscales differ at the free surface with the u_1 component scale larger and the u_2 component scale smaller by the same amounts than their closed channel centerline values.

The vertical macroscale, Λ_{2j}, is given by:

$$\Lambda_{2j}(x_2) = \int_0^1 R_{jj}(0,0,x_2,x_2')dx_2'. \qquad (9)$$

At a given vertical location x_2, Λ_2 gives a measure of the vertical size of a typical eddy that can exist at that depth. These results are shown in Fig. 6. It is observed that Λ_{21} and Λ_{22} increase continuously away from the solid wall until approximately $x_2 = 0.6$, where the free surface effects become evident as both decrease. Generally speaking, both the free surface and solid boundaries have similar overall effects in that the eddy size that can exist there is smaller than that existing away from the boundary. However, the lack of viscous dissipation near the free surface apparently allows for a somewhat greater vertical extent than that found near a solid wall, as one would expect. The Λ_{23} macroscale results may not be easily interpreted near the solid boundary since $R_{33}(x_2, x_2')$ becomes negative there, presumably due to the presence of the counter-rotating vortex structure typically associated with the wall layer. Near the free surface however, $R_{33}(x_2, x_2')$ is strictly positive so that the interpretation of Λ_{23} as a length scale is more meaningful. As with the other two vertical macroscale components, the proximity of the free surface (or perhaps boundary in general) evidences itself as a decrease in the Λ_{23} scale. These results generally tend to confirm the HG model prediction of a strong truncation of the vertical extent of a typical eddy near the free surface.

To summarize, the macroscale results are particularly useful in understanding the change in shape of a typical eddy as it interacts with the free surface. Predominantly, the free surface effects relative to the closed channel centerline behavior are larger spanwise scales associated with the streamwise velocity component u_1; generally smaller streamwise and spanwise scales for the wall normal velocity component u_2; and larger streamwise scales associated with the spanwise velocity component u_3. Additionally, the vertical macroscales, Λ_{2j}, associated with all three velocity components decrease on approach to the free surface. This presents a reasonably clear picture of eddies which flatten out or become pancake-like in the horizontal plane as they undergo a reduction in their vertical extent. This is certainly in agreement with one's intuitive expectation of the similar effect of a solid boundary on an impinging eddy. These results indicate a streamwise stretching by a factor of about three and a spanwise elongation of approximately two.

It does not seem possible to make a quantitative comparison of these results with the HG model in its present form, since their model does not account for the strong anisotropy of the open channel flow studied here. Obviously there is some difficulty in defining a far-field integral length scale in this flow, whereas this scale is well defined for homogeneous turbulence. However, since the source layer of the HG model is generated by the no mass-flux boundary condition, it would seem that the scales of u_2 should give the best indication of the extent of free surface effects. In Fig. 7 the mean-square turbulence intensities scaled by the local turbulent kinetic energy are shown. This demonstrates clearly that all three velocity components show the effects of surface proximity at a distance of about $\Delta x_2 = 0.3$. (See Swean *et al.*[10] for a discussion of the redistribtion of energy from the vertical velocity component to both the streamwise and spanwise components.) Indeed the vertical velocity component is the only one which has associated macroscales of about this size and which are *smaller* than the macroscales at the centerline of the closed channel flow. This seems to indicate that the length scales for u_2 also determine the extent of the source layer. This result is certainly consistent with the source layer model of HG as noted above.

5. WALL-LAYER STREAK SPACING

In Section 3 the persistence of a spanwise periodic structure at relatively large distance away from the wall was noted for the open channel flow. These streamwise-elongated structures, commonly referred to as wall-layer streaks, appear in flow visualization studies as regions of low-speed fluid close to wall. Though there remains some controversy as to the significance of the streaks, there appears to be increasing evidence that they are indicators of quasi-streamwise oriented vortices. These vortices in turn are thought to play a role in the production of new turbulence and in Reynolds stress production. They were first observed experimentally by Hama (see Corrsin[13]) and later studied in more detail by Kline *et al.*[14]. Their visualization studies showed that the streaks were typically observed below $x_2^+ = 30$ and that they occurred randomly in space and time. Kline *et al.* also found that the average spanwise spacing between the streaks, $\overline{\lambda^+}$, was approximately 100 essentially independent of Reynolds number. The experimental results reported by Nakagawa and Nezu[15] for open channel flow indicate that the mean streak spacing increases with distance from the wall and ultimately approaches a value of $\overline{\lambda^+} \approx 2x_2^+$ for $x_2^+ \geq 50$. This led them to speculate that the increase in length scale resulted from a coalescence (similar to the pairing interaction observed in free shear flows) of neighboring low-speed streaks as the distance from the wall increases. However, it should be noted that for the locations above $x_2^+ > 30$ the spanwise length scale they observe is very weak and may not necessarily correspond to well-defined streaks.

More recently, Smith and Metzler[16], in agreement with the findings of Nakagawa and Nezu, found that the average spanwise wavelength increased from

93 at $x_2^+ = 1$ to 146 at $x_2^+ = 30$. They noted, however, that beyond $x_2^+ = 30$ that the streaks were not sufficiently well defined to warrant making streak counts and they suggest that $x_2^+ \approx 40$ is the upper limit for which extended regions of low-speed fluid continue to exist. Also in agreement with Nakagawa and Nezu, they found that streak coalescence in the region $10 \leq x_2^+ \leq 30$ contributed to the increasingly disrupted streak pattern and overall increase in the spanwise length scale with distance from the wall. They noted that since the most active merging occurs in the region of maximum turbulent energy production, this merging process may very well be important to the turbulence production cycle. The observation of wall-layer streaks has not been confined strictly to experimental studies; various numerical simulations appear to very satisfactorily capture the wall-layer dynamics. As an example, KMM show very good agreement with the experimental determinations of the variation of mean spanwise streak spacing with distance from the wall.

In Fig. 8 the dependence of the mean streak spacing on x_2^+ is presented for both open and closed channel flows along with various experimental and numerical simulation results. Here the mean streak spacing is defined as twice the spanwise distance at which $R_{11}(\Delta x_3)$ reaches a minimum (note that this definition of $\overline{\lambda^+}$ is consistent with KMM). The results indicate clearly that for $x_2^+ < 12$ there is excellent agreement among all the studies that $\overline{\lambda^+} \simeq 100$. The streak spacing in the open channel case shows a jump from a value of 105 at $x_2^+ = 12$ to approximately 130 at $x_2^+ = 15$. Farther from the wall, the open channel streak spacing increases at a rate which is roughly the same as in the closed channel but always remains larger. Thus, Fig. 8 shows that at $x_2^+ \simeq 65$, $\overline{\lambda^+}$ has attained a value roughly twice twice that observed at $x_2^+ \simeq 12$. It is also clear that, unlike the closed channel case where the streak spacing is apparently only clearly defined out to perhaps $x_2^+ \simeq 50$, the spanwise periodic streaks can definitely be observed well out to $x_2^+ \simeq 80$ in the open channel flow. This is in fact within the logarithmic layer of the streamwise velocity profile (see Swean *et al.*[10] for the open channel flow mean velocity profile). It is apparent that the the streaky structure in open channel turbulence is both larger in scale and persists farther from the wall than in closed channel turbulence.

Though the reasons for these differences are far from evident, a few speculations are now offered to explain this behavior. The only obvious difference between these two flow fields is the boundary condition imposed on the upper boundary. Since the shear-free boundary suppresses the production of new turbulence we can envision that this must in turn suppress the ejection of low momentum fluid that would otherwise occur if the boundary were rigid (i.e no-slip boundary conditions). The suppression of these ejections from the top boundary (free surface) toward the bottom boundary (solid wall) may be responsible for slowing down the production of turbulence by lowering the probability of shear layer formation in the region of the solid wall. Thus, the larger, more coherent streaks near the wall in open channel turbulence are due to the suppression of turbulence production at the free surface. Furthermore, in boundary layer flows the entrainment of outer irrotaional fluid may act like ejections from the upper wall of a channel. In this sense, boundary layer flow has a closer resemblance to closed channel flow than to open channel flow. These results suggest that the outer flow does have an effect on the wall region at least at these low Reynolds numbers.

6. CONCLUSIONS

The structure of turbulence near a free surface has been studied using the results of a direct simulation. The method employed here to understand this structure is to compare the open channel turbulence results with its well studied closed channel turbulence counterpart. A comparative examination of the turbulent macroscales and microscales in these two cases reveals a significant flattening of a typical eddy near the free surface. This flattening is evidenced by a notably larger streamwise scale associated with the spanwise velocity component and a comensurately larger spanwise scale of the streamwise velocity component. Additionally, the vertical macroscales for all three velocity components are smaller than the companion closed channel values. In this flow, the source layer described by the Hunt-Graham model appears to extend about 0.3 channel heights below the free surface. This source region seems to correlate most strongly with the structure of the vertical component of velocity. All length scales for this component are about the correct size and all are smaller than the macroscales at the centerline of the closed channel flow. A direct quantitative comparison of these results with the HG model is not possible since the model does account for the strong anisotropy of the turbulence present in this flow. The energy spectra for all three components of velocity are in qualitative agreement with the HG model though resolution effects and anisotropy limit direct quantitative comparison.

An interesting phenomenon revealed by the current study is the increase in size and persistence of the spanwise periodic structure near the wall. In open channel turbulence this structure is larger in scale and penetrates farther into the flow than in closed channel turbulent flow. The origin of this effect is not clear but one possible explanation is that the free surface suppresses interactions which would normally occur

between the no-slip boundaries of channel flow. This observation lends support to the possibility that the outer flow has a significant effect on wall layer structure. In future work, a quantitative comparison of these results with a modified form of the HG model will be attempted and higher resolution simulations will be undertaken to further elucidate the structure of the turbulence near the free surface.

ACKNOWLEDGEMENTS

This work is supported by the Naval Research Laboratory under the Fluid Dynamics Task Area and the Office of Naval Research under the Surface Ship Wake Detection Program. Many of the calculations were performed under an NRL Cray Grant. The authors acknowledge the many fruitful discussions with Dr. J.D. Crouch.

REFERENCES

[1]Uzkan, T. and Reynolds, W.C., "A Shear-Free Turbulent Boundary Layer," *Journal of Fluid Mechanics*, Vol. 28, 1967, pp. 803-821.

[2]Thomas, N.H. and Hancock, P.E., "Grid Turbulence Near a Moving Wall," *Journal of Fluid Mechanics*, Vol. 82, 1977, pp. 481-496.

[3]Hunt, J.C.R. and Graham, J.M.R., "Free Stream Turbulence Near Plane Boundaries," *Journal of Fluid Mechanics*, Vol. 84, 1978, pp. 209-235.

[4]Biringen, S. and Reynolds, W.C., "Large-Eddy Simulation of the Shear-Free Turbulent Boundary Layer," *Journal of Fluid Mechanics*, Vol. 103, 1981, pp. 53-63.

[5]Brumley, B.H. and Jirka, G.H., "Near-Surface Turbulence in a Grid-Stirred Tank," *Journal of Fluid Mechanics*, Vol. 183, 1987, pp. 235-263.

[6]Orszag, S.A. and Patera, A.T., "Subcritical Transition to Turbulence in Planar Shear Flows," in *Transition and Turbulence*, ed. by R.E. Myer, Academic, 1981, pp. 127-146.

[7]Kim, J., Moin, P., and Moser, R., "Turbulence Statistics in a Fully Developed Channel Flow at Low Reynolds Number," *Journal of Fluid Mechanics*, Vol. 177, 1987, pp. 133-166.

[8]Leighton, R.I., Swean, T.F., Jr., Handler, R.A., and Swearingen, J.D., "Direct Simulation of Low Reynolds Number Open Channel Flow," NRL Memorandum Report, 1991.

[9]Komori, S., Ueda H., Ogino, F., and Mizushina, T., "Turbulence Structure and Transport Mechanism at the Free Surface in an Open Channel Flow," *International Journal of Heat and Mass Transfer*, Vol. 25, 1982, pp. 513-521.

[10]Swean, T.F., Jr., Leighton, R.I., Handler, R.A., and Swearingen, J.D., "Turbulence Modeling Near the Free Surface in and Open Channel Flow," AIAA Paper 91-0613, 29th Aerospace Sciences Meeting, Jan. 7-10, 1991, Reno, Nevada.

[11] Sirovich, L. "Turbulence and the Dynamics Coherent Structures: Part II: Symmetries and Transformations," *Quarterly of Applied Mathematics*, Vol. 45, 1987, pp. 573-582.

[12]Hinze, J.O., *Turbulence*, McGraw-Hill, New York, 1975.

[13] Corrsin, S., "Some Current Problems in Turbulent Shear Flows," *Symposium on Naval Hydrodynamics*, Publication 515, National Academy of Sciences-National Research Council, 1957, pp. 373-407.

[14]Kline, S.J., Reynolds, W.C., Schraub, F.A., and Runstadler, P.W., "The Structure of Turbulent Boundary Layers," *Journal of Fluid Mechanics*, Vol. 30, 1967, pp. 741-773.

[15]Nakagawa, H. and Nezu, I., "Structure of Space-Time Correlations of Bursting Phenomena in an Open-Channel Flow," *Journal of Fluid Mechanics*, Vol. 104, 1981, pp. 1-43.

[16]Smith, C.R. and Metzler, S.P., "The Characteristics of Low-Speed Streaks in the Near-Wall Region of a Turbulent Boundary Layer," *Journal of Fluid Mechanics*, Vol. 129, 1983, pp. 27-54.

[17]Schraub, F.A. and Kline, S.J., "A Study of the Structure of the Turbulent Boundary Layer With and Without Longitudinal Pressure Gradients," *Department of Mechanical Engineering Report* MD-12, 1965, Stanford University.

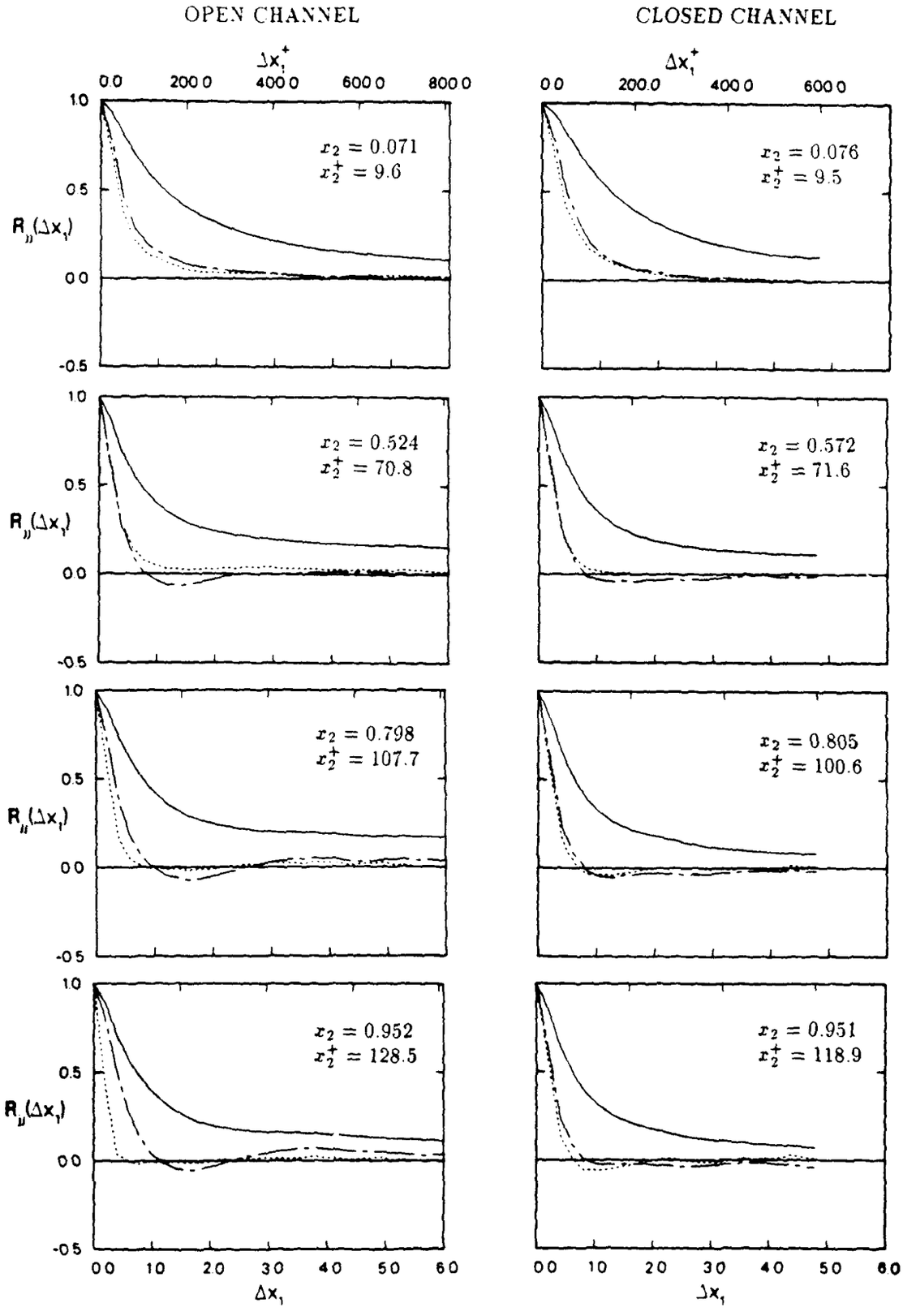

Fig. 1 Streamwise two-point correlations: ———, R_{11}; – – – –, R_{22}; — – — –, R_{33}.

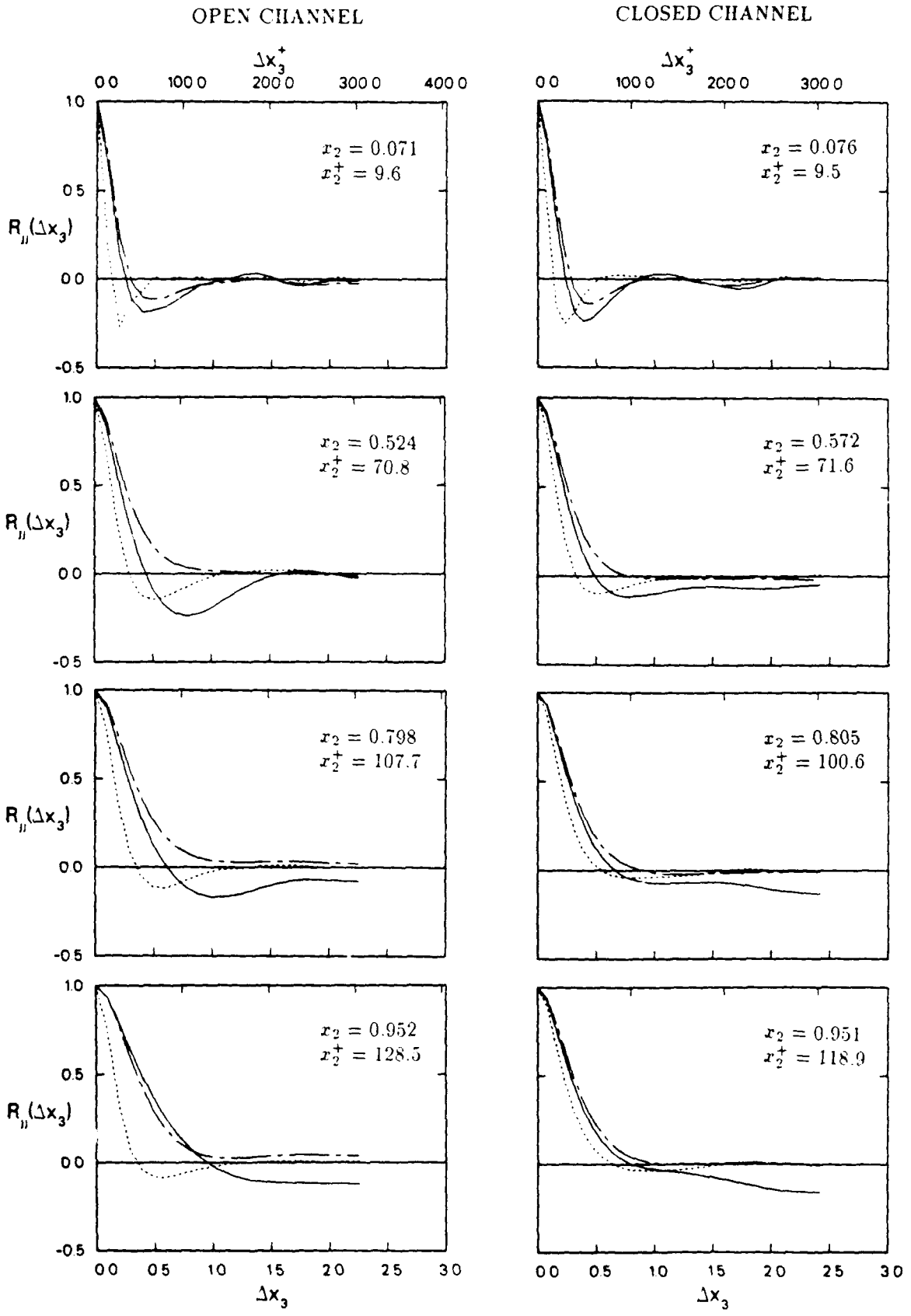

Fig. 2 Spanwise two-point correlations: ——, R_{11}; - - - -, R_{22}; — - —, R_{33}.

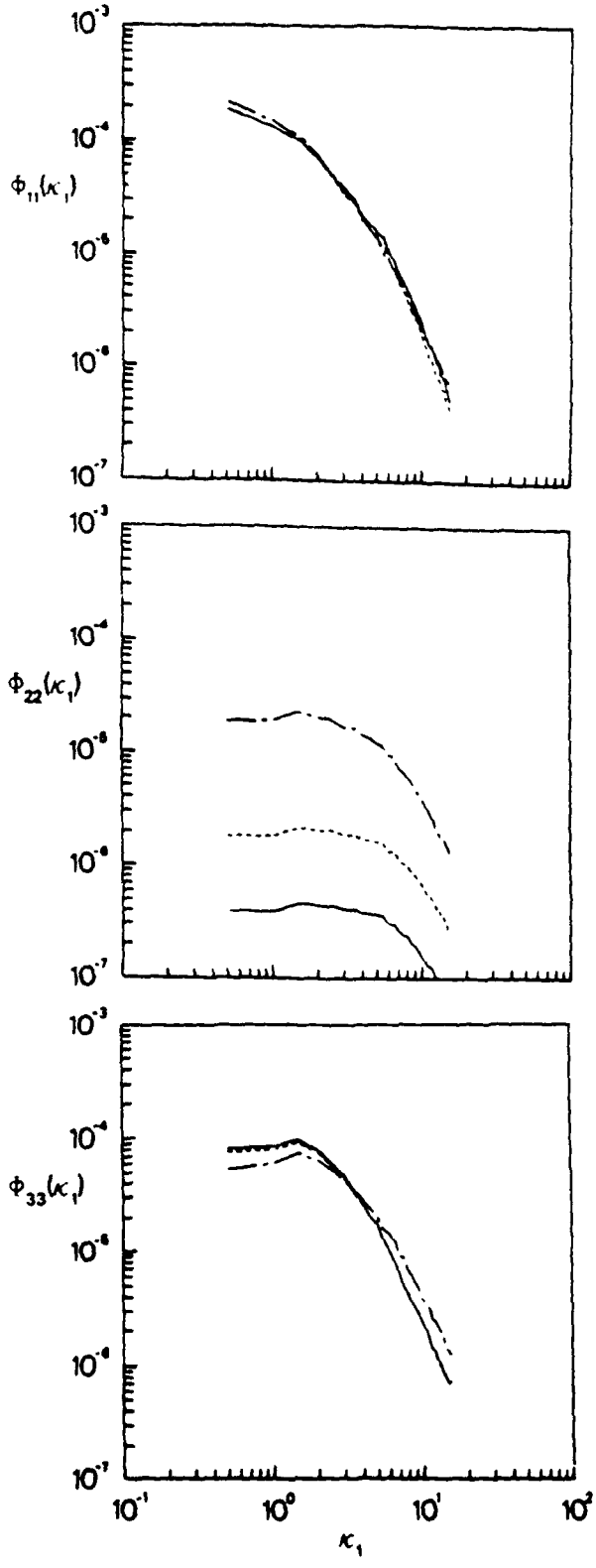

Fig. 3 Velocity spectra near the free surface: ———, $x_2 = 0.978$; – – – –, $x_2 = 0.952$; —— —, $x_2 = 0.798$.

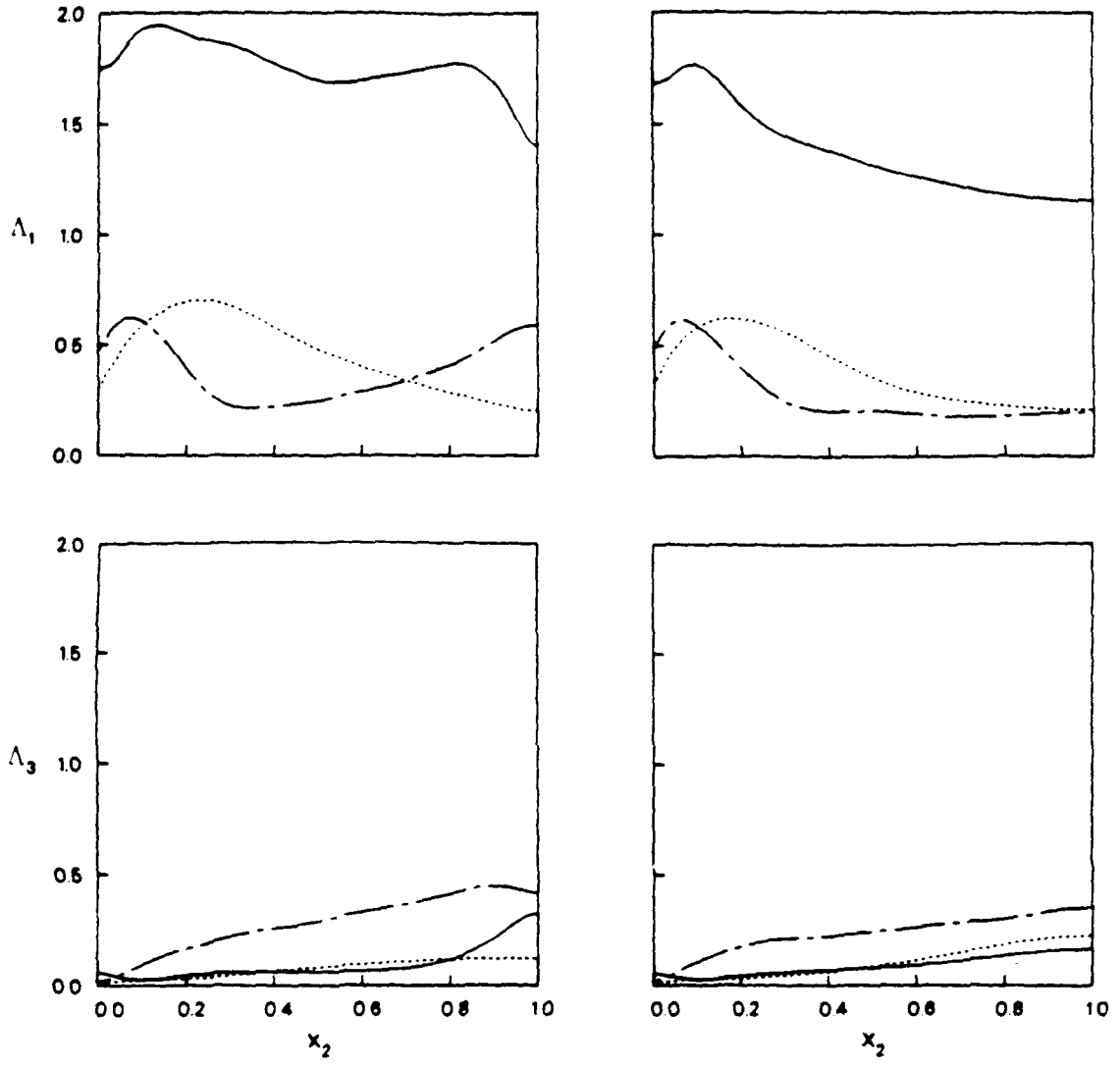

Fig. 4 Streamwise and spanwise macroscales: ———, Λ_{11}; – – – –, Λ_{12}; — – — –, Λ_{13}.

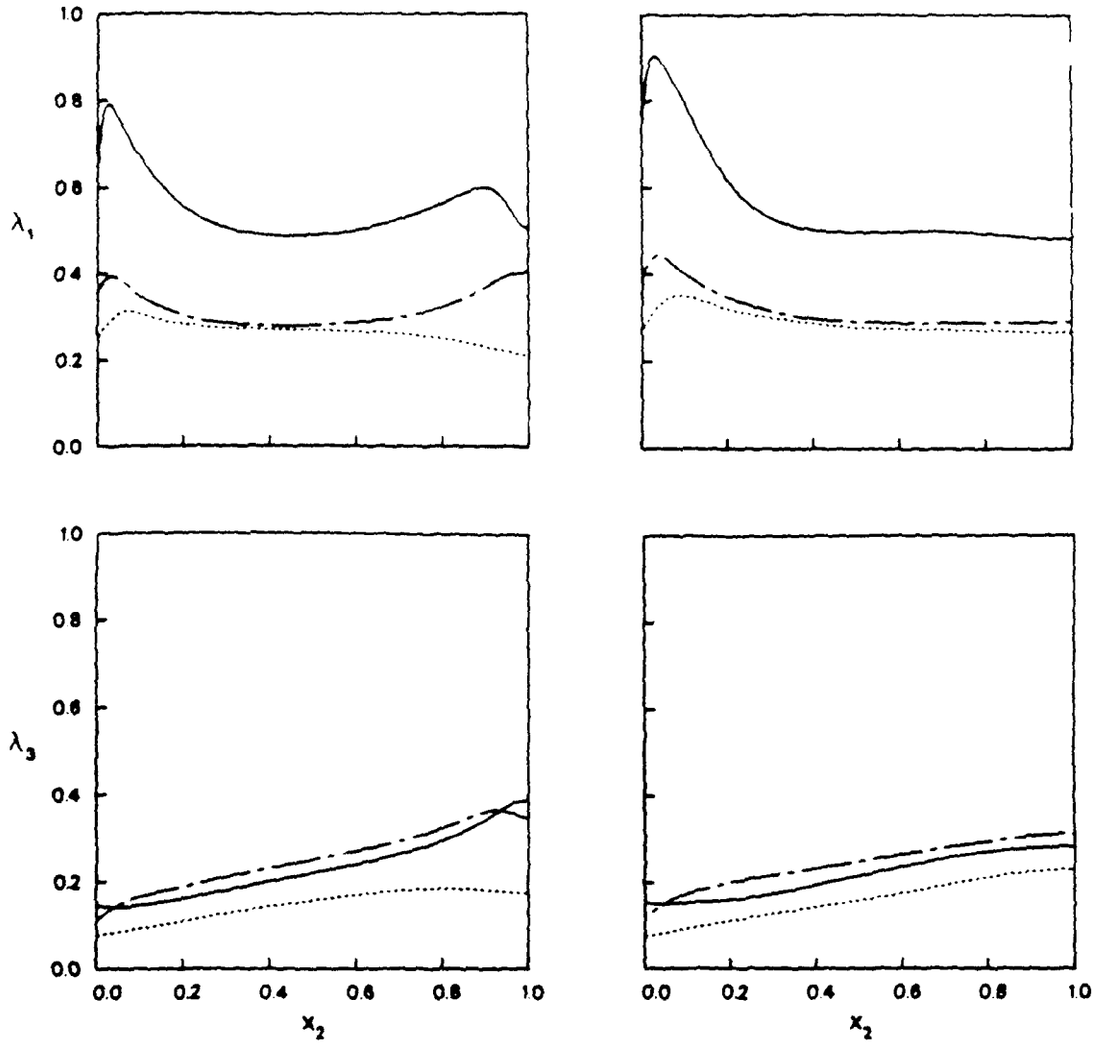

Fig. 5 Streamwise and spanwise microscales: ———, λ_{i1}; – – – –, λ_{i2}; — · —, λ_{i3}.

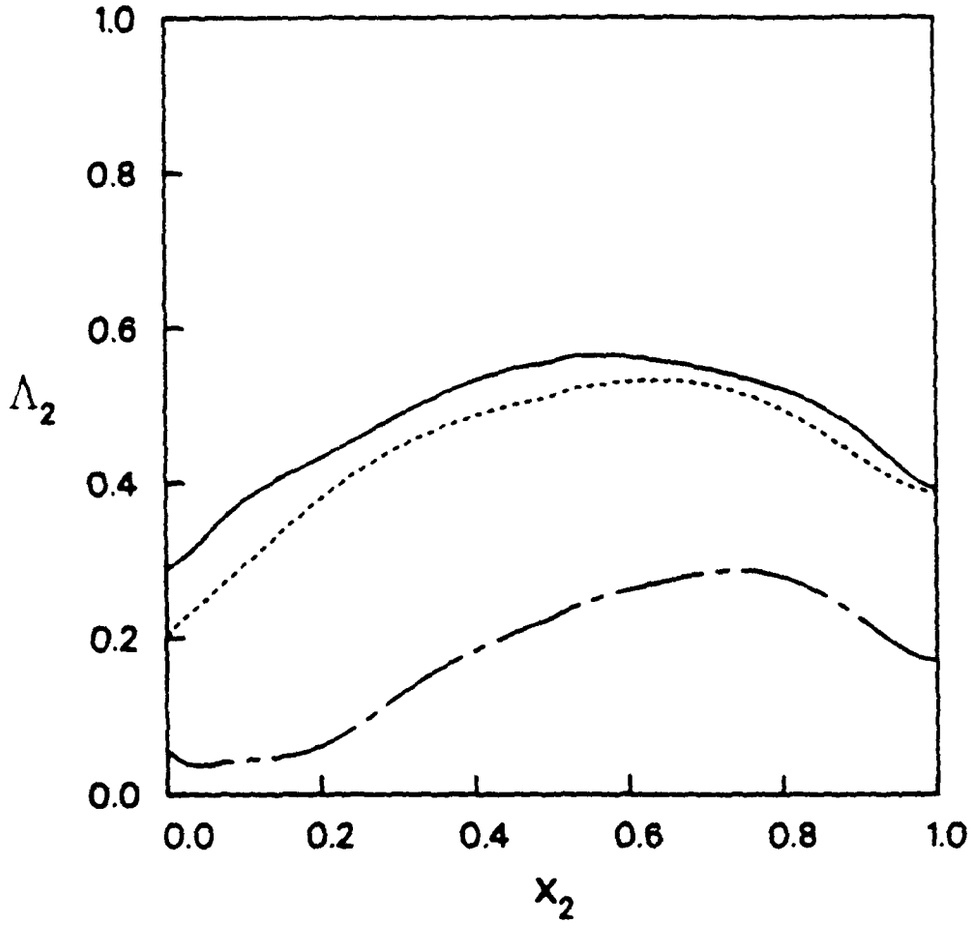

Fig. 6 Vertical macroscales: ——, Λ_{21}; – – – –, Λ_{22}; — — —, Λ_{23}.

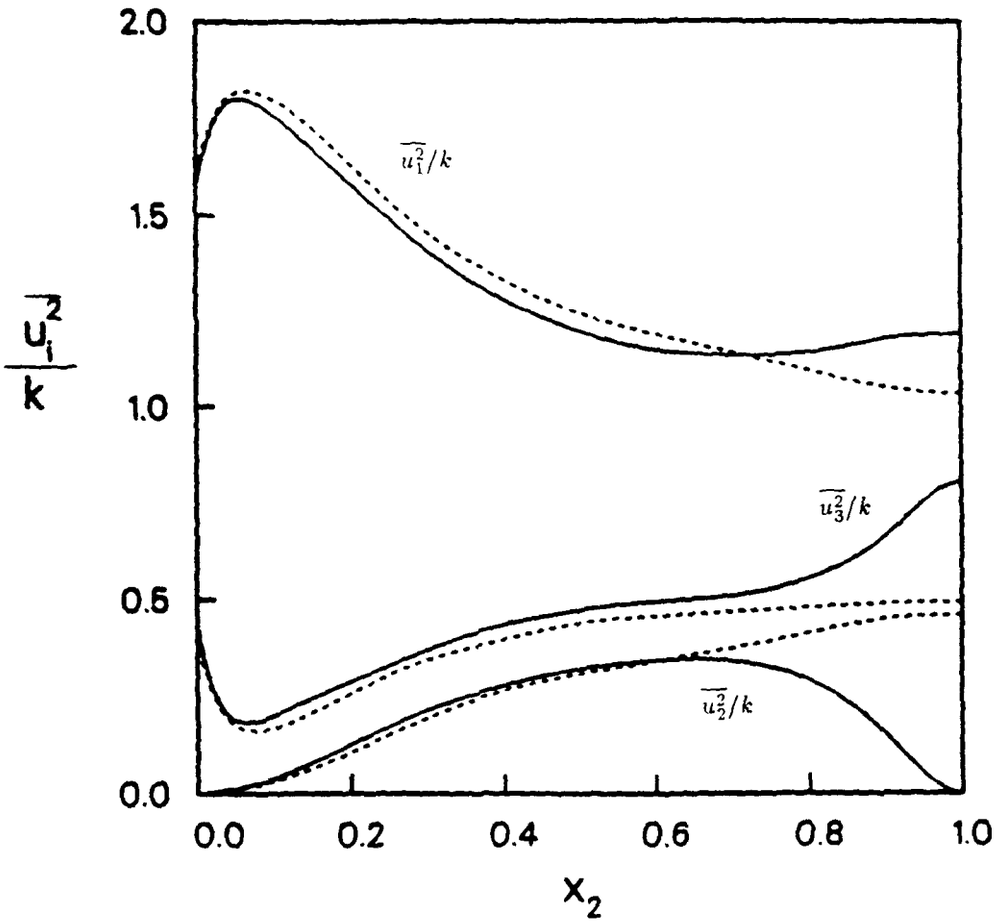

Fig. 7 Profiles of normal stresses scaled by the local value of turbulence kinetic energy. Dashed lines are for the closed channel simulation.

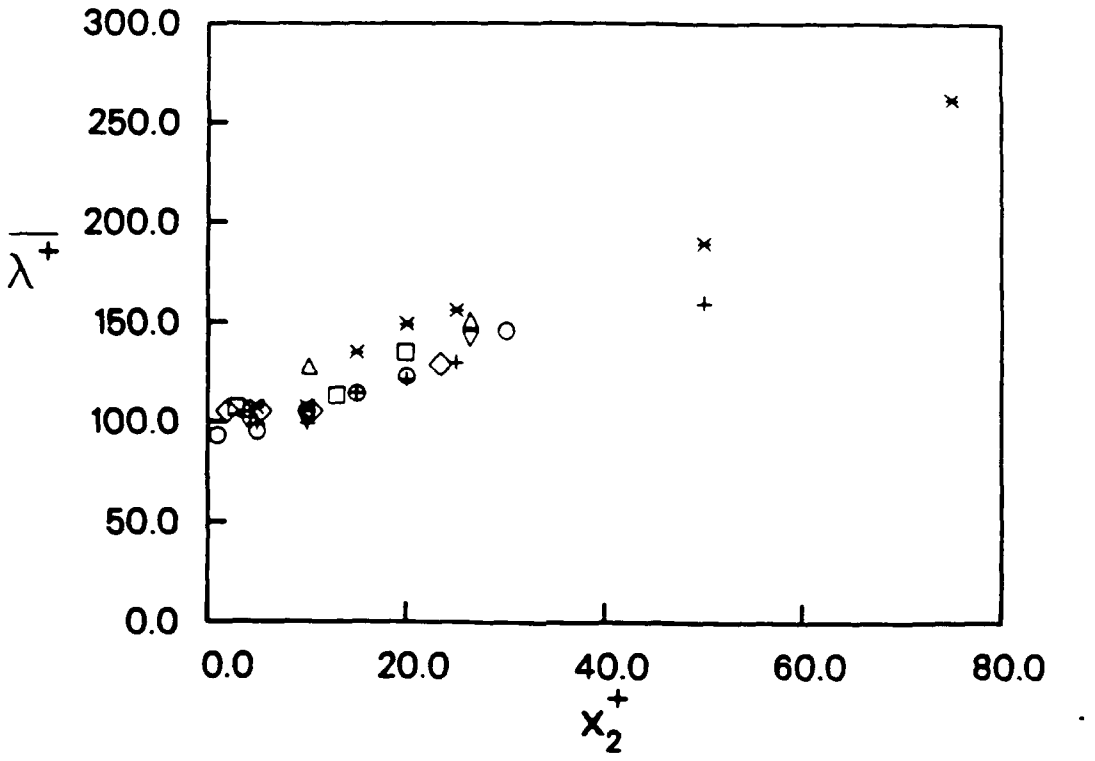

Fig. 8 Variation of mean spanwise streak spacing with wall normal distance. Present study: ⁎, open channel, $R^* = 135$; +, closed channel, $R^* = 125$. Smith and Metzler[16]: o, boundary layer expt., $R_\theta = 2030$. Schraub and Kline[17]: □, boundary layer expt., $R_\theta = 1325$. Nakagawa and Nezu[15]: open channel expt., ▽, $R^* = 248$; △, $R^* = 378$. Kim, Moin, and Moser[7]: ◇, closed channel simulation, $R^* = 180$.